International Journal of Engineering Research
Volume No.3, Issue No.7, pp : 430-434
ISSN:2319-6890)(online),2347-5013(print)
01 July 2014

CFD Analysis on Airfoil at High Angles of Attack

Dr.P.PrabhakaraRao[1] & Sri Sampath.V[2]
Department of Mechanical Engineering,Kakatiya Institute of Technology& Science Warangal-506015
[1]chantifft@rediffmail.com ,[2]sampath_velpula@yahoo.com

Abstract— ***The present work describes a conceptual study of performance enhancing devices for an airfoil by using Computational Fluid Dynamics. Two simple passive devices are selected and examined for Lift improvement and for decrease in Drag. The motivation behind this project is to study these effective techniques to improve performance with fewer drawbacks then previously existing model. The effective position for the location of Dimples and Cylinder are found out. Among the two selected models, Dimple model shows good results compare to other. The CAD model is prepared in CATIA V5 R19, pre-processing is done in ANSYS ICEM CFD 14.0 and simulations are carried out in ANSYS FLUENT 14.0. The overall aim of the project is to improve airfoil performance at high angle-of-attack. The results justify the optimum position for placing Dimple and cylinder for enhancing airfoil performance.***

Keywords—**Airfoil, Angle of attack, Coefficient of lift, dimple.**

I. Introduction

The aerodynamic cross section of a body such as a wing that creates lift as it moves through air or fluid is called as an airfoil or aero foil. An airfoil-shaped body moved through a fluid produces an aerodynamic force. The component of this force perpendicular to the direction of motion is called lift. The component parallel to the direction of motion is called drag[I].

The lift on an airfoil is primarily the result of its angle of attack and shape. When oriented at a suitable angle, the airfoil deflects the oncoming air, resulting in a force on the airfoil in the direction opposite to the deflection. This force is known as aerodynamic force and can be resolved into two components: Lift and drag. Most foil shapes require a positive angle of attack to generate lift, but cambered airfoils can generate lift at zero angle of attack. This "turning" of the air in the vicinity of the airfoil creates curved streamlines which results in lower pressure on one side and higher pressure on the other[II]. This pressure difference is accompanied by a velocity difference, via Bernoulli's principle, so the resulting flow field about the airfoil has a higher average velocity on the upper surface than on the lower surface.

1.1 Aerodynamic Forces

The aerodynamic forces and moments on a body are due to two basic sources:

1. Pressure distribution over the body surface
2. Shear stress distribution over the body surface

No matter how complex the body shape maybe, the aerodynamic forces and moments on the body are entirely due to the above two basic sources. The only mechanisms nature has for communicating a force to a body moving through a fluid are pressure and shear stress distributions on the body surface. The pressure p, acts normal to the surface and the shear stress τ, acts tangential to the surface[III].

1.2 Flow Control

The purposes of aircraft flow manipulation, as Gad-el-Hak [IV] explains, are: increasing lift, reducing drag and enhancing the mixing of mass, momentum and energy.In order to meet these objectives. 1.The laminar to turbulent transition has to be postponed or provoked, 2.The flow separation has to be avoided or initiated, 3.The flow turbulence has to be prevented or encouraged. All these seemingly contradictory goals are interrelated. It is not difficult to look only one performance target, the challenge is to consider the side effects and how to minimize them. Furthermore, it is essential that the resulting performance enhancing devices are simple, inexpensive and easy to operate**.** The net effect of the p and τ distributions integrated over the complete body surface is a resultant aerodynamic force and a moment. In turn, the resultant force can be split into two components, lift and drag.

1.3 Lift

The force lift, or simply lift, is a mechanical force generated by solid objects as they move through a fluid. While many types of objects can generate lift, the most common and familiar object in this category is the airfoil. Lift is the sum of all the fluid dynamic forces on a body perpendicular to the direction of the external flow approaching that body[V].

II. METHODOLOGY

2.1GEOMETRY GENERATION

Geometry of NACA 4412 is modeled in CATIA V5 R20, that can be read into FLUENT and other analysis software. An outline for the CATIA geometry creation process can be seen in Figure 2.1

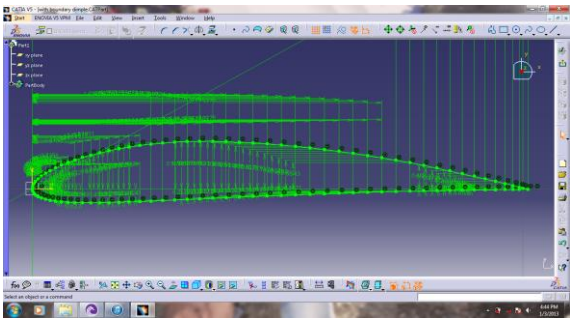

Figure21: Airfoil geometry created in CATIA

2.2Grid Generation

Approximations are used to solve the governing differential equations of fluid mechanics. This is accomplished by converting partial derivatives to a finite difference form. These finite difference equations, also known as approximate algebraic equations, are solved at discrete points inside the

ISSN:2319-6890)(online),2347-5013(print)
01 July 2014

domain of interest. Hence, a set of grid points need to be defined within the boundaries of the domain[VI].

Generally, a domain has a rectangular shape where grid points are assigned to each grid line, making grid points easier to be identified. This domain is called a structured grid or a rectangular mesh (If 2D). On the other hand, grid points can be generated in a less orderly manner. This domain is known as an unstructured grid or triangular mesh (If 2D). In order to obtain more accurate results in the boundary layer , a dense or fine mesh is necessary to calculate viscous shear layer behavior (y+ =1). However, a fine mesh throughout the domain causes an increase in grid points, and eventually the CPU time. It is recommended to tailor the grid size near the wall to add precision. This process is referred to as clustering, which is easier to implement by using structured mesh.

A commercial grid generator ANSYS ICEM CFD is used to mesh our domain. Shown in Fig 2.2 presents the single element **NACA 4412** domain as it extends 20 chord lengths downstream and 13 chord lengths to the sides and upstream. A two – dimensional structured C-Grid domain is applied in x-y direction, which consist around 1,00,000 grid points. TO increase the grid points at the surface of the wall, highly skewed mesh generation is inevitable.

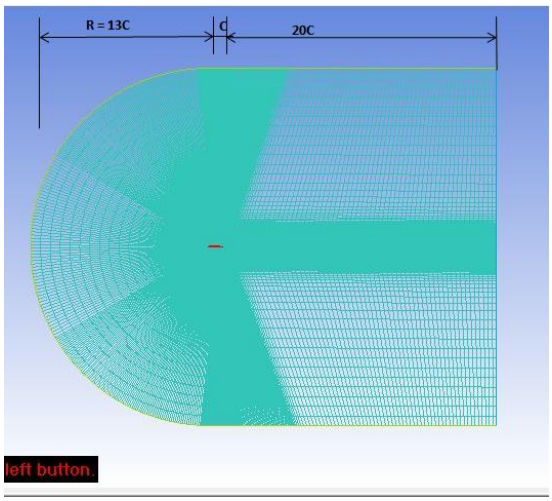

Figure 2.2: Single element airfoil domain size and clustering

III. RESULTS

For each model, several factors, at different possible values or levels, need to be examined. This may lead to infinite simulation time and cost. Using factorial design on Design of Experiment methods, introduced by Montgomery, the numbers of combinations are reduced. In this study, two or three primary factors (e.g., x and y locations), and several angles of attack are commonly examined.

3.1Dimples

The device analysis matrix for the Dimple configuration is presented in table3.1. Two factors are considered to be most influential: x-location and d, as the diameter of the Dimple.

In addition to these two other models are also tested. Dimples are located before and after the maximum thickness of the airfoil so that laminar flow close to the leading edge is expected which is Shown in Fig 3.1 the model identifying the corresponding x and d arrangements.

Table 3.1: Analysis matrix for Dimple model

Model	**X**	**d**
A	0.75c	0.05c
B	0.25c	0.1c
C	0.75c	0.1c
D	0.25c	0.05c

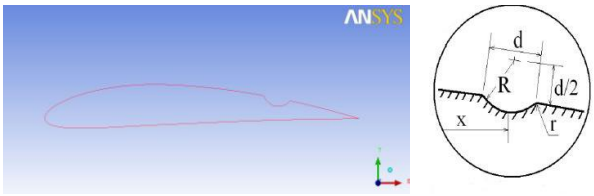

R=d, r = d / 10.

Figure 3.1: Closer View of Dimple

A total of four models are simulated at four angles-of-attack shown in tables 3.2 and 3.3. Section lift coefficient, (Cl) against angle of attack is plotted in Graph 3.1.Clearly as the Dimple moves towards trailing edge it shows good results. Meanwhile, dimples closer to the airfoil trailing edge have less significance when compared to other models. however, a slight improvement is observed in all other models. Section Drag coefficient (Cd) and Lift-to-drag ratio against angles-of-attack are shown below in Graphs (3.1 – 3.3). Further investigations need to be implemented to validate these results.

Table 3.2 : Result of Dimple at 0 and 5 degrees

Model	O degrees			5 degrees		
	Cl	Cd	Cl/cd	Cl	Cd	Cl/Cd
Base Line	6.93E-05	5.91E-05	1.17	4.42E-04	8.30E-04	5.33
Mod-A	3.80E-03	2.30E-04	16.51	8.8.E-03	2.95E-04	29.87
Mod - B	3.32E-03	2.58E-04	12.851	7.94E-03	3.67E-04	29.61
Mod-C	3.63E-03	2.38E-04	15.22	8.43E-03	3.06E-04	27.5
Mod-D	3.33E-03	2.37E-04	14.054	7.83E-03	3.55E-04	22.061

Table 3.3: Results of Dimple at 10 and 15 degrees

Model	10 degrees			15 degrees		
	Cl	Cd	Cl/Cd	Cl	Cd	Cl/Cd
Base Line	6.78E-04	1.36E-04	4.98	7.84E-04	2.24E-04	3.5
Mod-A	1.28E-02	4.42E-04	28.89	1.23E-02	1.28e-03	9.658
Mod-B	1.604E-02	5.65E-04	28.36	1.15E-02	1.33e-03	22.38
Mod-C	1.215E-02	4.75E-04	25.60	1.22E-02	1.23e-03	9.91
Mod-D	1.16E-02	5.47E-04	21.24	1.17E-02	1.25e-03	9.32

Using the above tabulated values Graphs are plotted to determine the best model in terms of positioning of dimple. From the below graphs Model A shows best results in terms of

ISSN:2319-6890)(online),2347-5013(print)
01 July 2014

both co-efficient of lift and co-efficient of drag. It is observed that Model A is the best suited model for positing of Dimple.

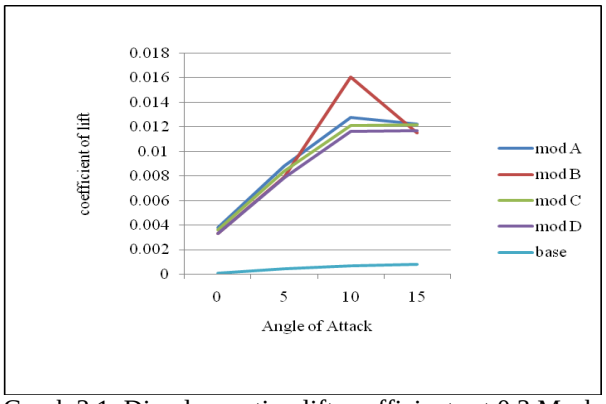

Graph 3.1: Dimples section lift coefficients at 0.3 Mach speed

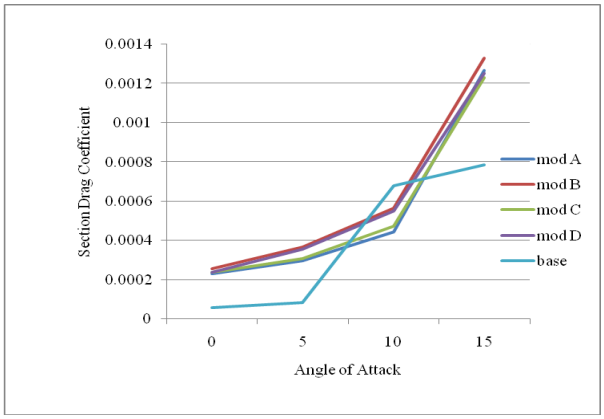

Graph3.2: Sections drag coefficients VS angle of attack

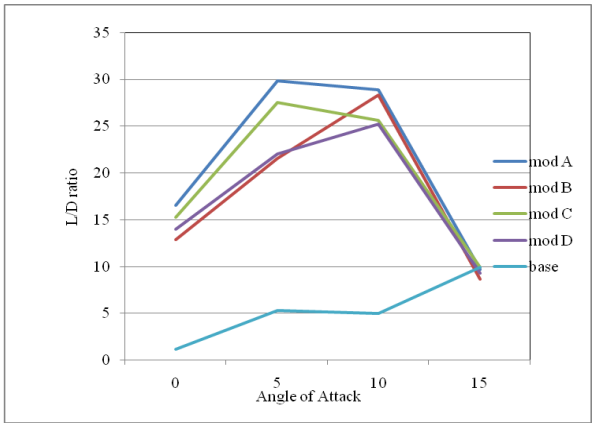

Graph 3.3: Lift-to-drag ratio VS angle of attack

The static pressure contours of all the models and the baseline airfoil are shown in Figures (3.2 –3.5).

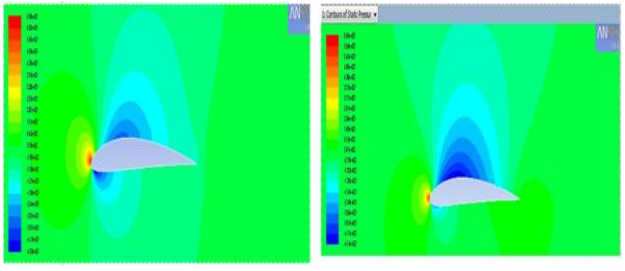

Figure 3.2: Static pressure contours of model A at AOA 0^0 degrees Vs base model at 0^0

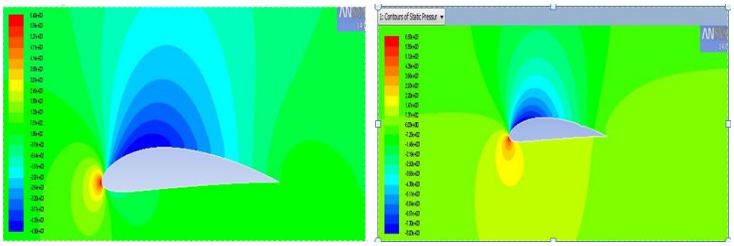

Figure 3.3: Static pressure contours of model A at angle of attack 5^0 degrees base model at 5^0

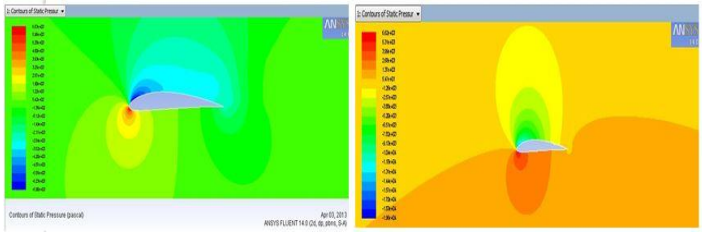

Figure 3.4: Static pressure contours of model A at angle of attack 10^0 degreesVs base model at 10^0

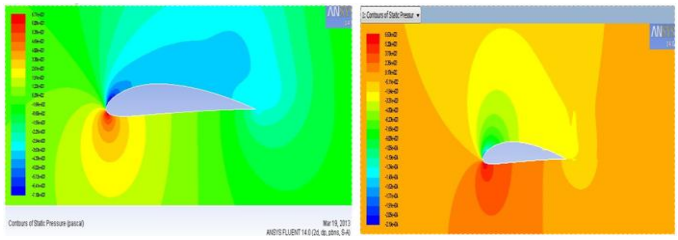

Figure3.5: Static pressure contours of model A at angle of attack 15^0 degrees Vs base model at 15^0

3.2 Cylinders

The device analysis matrix, for the cylinder concept, is shown in table 3.4. In contrast to the previous section, likely dependents for this configuration are not easy to identify. Hence, a trail-and-error method is utilized to show the model total Cl and Cd dependency. Figure 3.6 shows the model with corresponding X, Y and R arrangements, where (y) is the gap between the cylinder and the airfoil.

Table3.4: Analysis Matrix for Cylinder Model

Model	X	Y	y	R
A	0.4c	0.0970c	0.02c	0.01c
B	0.4c	0.0970c	0.02c	0.005c
C	0.3c	0.0988c	0.02c	0.005c
D	0.5c	0.091c	0.02c	0.005c
E	0.6c	0.077c	0.02c	0.005c

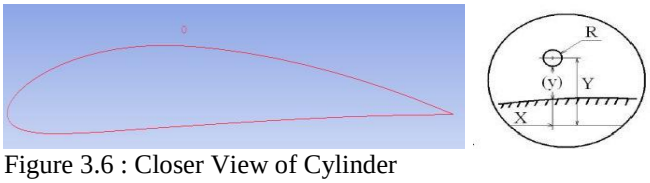

Figure 3.6 : Closer View of Cylinder

The cylinder diameter is tested for the first two models: A and B. Based on the results the superior model is

ISSN:2319-6890)(online),2347-5013(print)
01 July 2014

taken to the next assessment. Note that the cylinder radius has two different values of 0.005c and 0.01c.

A total of five models are simulated at three different angles-of-attack. In terms of all models. Model E gives better results. This can be seen from the below graphs. Model E does not have high lift coefficient compared to base model but there is a decrease in drag coefficient at high angle-of-attack. As the cylinder moves toward the trailing-edge, the lift coefficient improves. On the other hand, a large cylinder diameter and a smaller gap (y) have negative effects on the drag coefficient. The cylinder wake is not only causing an increase in drag but also initiating flow separation. This can be observed in pressure contours shown below in fig (3.7 –3.9). Further investigations are needed to be implemented to validate these results.Using the above tabulated values Graphs are plotted to determine the best model in terms of positioning of Cylinder. From the below graphs Model E shows best results in terms of both co-efficient of lift and co-efficient of drag. We observed that Model E is the best suited model for positing of Cylinder.

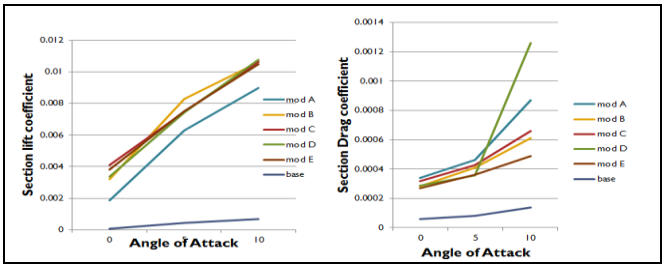

Graph3.4: Section lift and drag coefficient Vs angle of attack of cylinder model

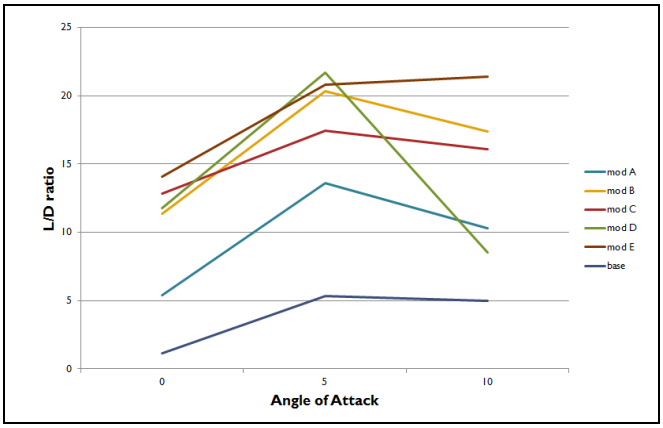

Graph3.5: lift to drag ratio coefficient Vs angle of attack of cylinder model

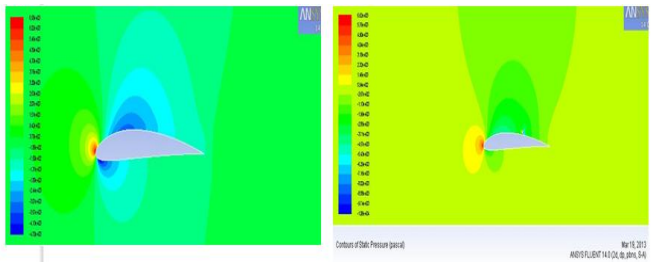

Figure 3.7 : static pressure contours of base 0^0Vs cylinder model E at angle of attack 0^0

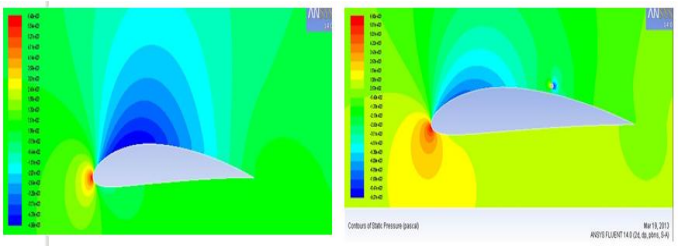

Figure 3.8: static pressure contours of base 5^0Vs cylinder model E at angle of attack 5^0

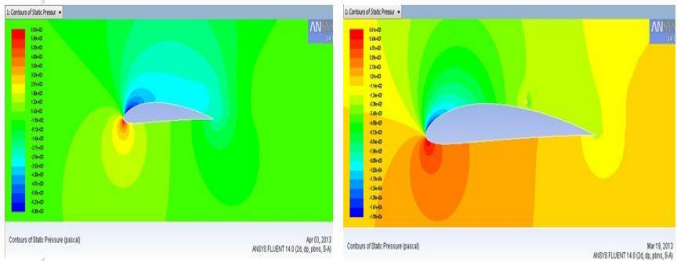

Figure 3.9: static pressure: contours of base 10^0Vs cylinder model E at angle of attack 10^0

IV. Conclusion

Two simple devices were tested, using Spalart-Allmaras (SA) turbulence model, to evaluate their effect on lift and drag coefficients. Results for each conceptual design were compared against a single-element airfoil. The cylinder model has the poorest results in terms of coefficient of lift and coefficient of drag Vs angle-of-attack. The pressure contours and graphs justify this conclusion. The dimple Model A is the best among other dimple configurations. As the dimple moves towards trailing-edge it shows improvement in parameters. The overall best model was the Dimple model A, where there are improvements in lift and drag coefficients. Further investigations are to be done to validate these results. Various parameters like flow separation, effect at high angles, turbulent viscosity ratio are to be considered in order to validate these results

References

i. *Gad-el-Hak, Flow Control Passive: Active and Reactive Flow Management, First ed., Cambridge University Press, 2000.*

ii. *D.J. Butter, "Recent Progress on Development and Understanding of High Lift Systems," in Improvement of Aerodynamic Performance Through Boundary Layer Control and High Lift Systems, Brussels, Belgium, pp. 1.1-1.26,1984.*

iii. *J.D. Anderson, Fundamentals of Aerodynamics, McGraw Hill Series, Third Edition, pp. 41-47, 2001.*

iv. *A.M.O. Smith, "High-Lift Aerodynamics," Journal of Aircraft vol. 12, pp. 501-530, 1975.*

v. *R.H. Liebeck, Smyth, D.N., "Study of slat-airfoil combinations using computer graphics," Journal of Aircraft, vol.10, April, pp. 254-256, 1973.*

vi. *M. Sajben, et al., "A New, Passive Boundary Layer Control Device," AIAA-1976-700, presented at the American Institute of Aeronautics and Astronautics and Society of Automotive Engineers, Propulsion Conference, 12th, Palo Alto, Calif, 26-29 July, 1976.*

vii. *F.G. Howard and W.L. Goodman, "Drag Reduction on a Bluff Body at Yaw Angles to 30 Degrees," Journal of Spacecraft and Rockets, vol. 24, pp. 179-181, 1987.*

viii. L. Hee-Chang and L. Sang-Joon, "Flow Control of Circular Cylinders with Longitudinal Grooved Surfaces," AIAA Journal, vol. 40, pp.2027-36, 2002.

ix. R.A. Wallis, "Wind Tunnel Studies of Leading Edge Separation Phenomena on a Quarter Scale Model of the Outer Panel of the Handley Page Victor Wing with and without Nose Droop," R&M 3455, 1965.

x. J.J. Bertin, Aerodynamics for Engineers, 4th ed., prentice Hall, pp. 134-136, 2002.

xi. J.C. Lin, "Control of Turbulent Boundary-Layer separation using Micro-Vortex Generators," AIAA-1999-3404, presented at the 30th AIAA Fluid Dynamics Conference, Norfolk, VA, 1999.

xii. M.P. Patel and T.S. e.a. Prince, "Control of Aircraft Stall via Embedded Pressure Sensors and Deployable Flow Effectors," AIAA-2002-3170, presented at the 1st Flow Control Conference, Jun 24-26 2002, St. Louis, Missouri, 2002.